HEFAT2011
8th International Conference on Heat Transfer, Fluid Mechanics and Thermodynamics
11–13 July 2011
Pointe Aux Piments, Mauritius

NUMERICAL SIMULATION OF UNSTEADY FLOWS WITH STRONG SHOCKS USING ADAPTIVE UNSTRUCTURED MESHES

Isola D. and Guardone A.*
*Author for correspondence
Dipartimento di Ingegneria Aerospaziale
Politecnico di Milano
Via La Masa 34, 20156 Milano,
Italy,
E-mail: isola@aero.polimi.it

ABSTRACT

In the present work numerical simulations of unsteady flows with moving shocks are presented. An unsteady mesh adaptation method, based on error equidistribution criteria, is adopted to capture the most important flow features. The modifications to the topology of the grid are locally interpreted in terms of continuous deformation of the finite volumes built around the nodes. The Arbitrary Lagrangian Eulerian formulation of the Euler equations is then apply to compute the flow variable over the new grid without resorting to any explicit interpolation step. The numerical results shows an increase in the accuracy of the solution, together with a strong reduction of the computational costs, with respect to uniform-grid computations using a larger number of nodes.

NOMENCLATURE

ρ	Density of mass
$\boldsymbol{m}$	Linear momentum vector
E^{t}	Total energy per unit volume
P	Pressure
M	Mach number
u	Conservative variables, $\mathsf{u} = (\rho, \boldsymbol{m}, E^{\mathrm{t}})^{\mathrm{T}}$
Ω	Computational domain
$\mathcal{C}$,$\partial\mathcal{C}$	Cell and cell boundary
$\boldsymbol{n}$, $\boldsymbol{\tau}$	Cell normal and tangent versor
$\boldsymbol{\eta}$, $\boldsymbol{\xi}$	Normal integrated vectors
$\boldsymbol{v}$	Interface velocity of the interface
ν	Integrated normal interface velocity
Φ	Numerical fluxes along the interface
u_∂	Boundary state function
V	Cell volume
V_{ik},$V_{i,\partial}$	Swept volume
$\mathbf{f}$	Two-dimensional Euler fluxes
I^n	$n \times n$ identity matrix
t	Time
$\mathcal{E}$	Set of elements of the triangulation
$\mathcal{K}$	Set of all nodes of the triangulation
$\mathcal{K}_{i,\neq}$	Set of nodes surrounding the i-th node
h_i	Cell circumscribing circle radius
$\boldsymbol{m}_\tau$, $\boldsymbol{m}_n$	tangent/normal versor to $\boldsymbol{m}$
$\mu(x)$	Average value of x
$\sigma(x)$	Standard deviation of x
$\mathcal{H}(x)$	Discrete Hessian matrix

INTRODUCTION

The unsteadiness of the flow field due to the propagation of shock waves results in dynamic loads that are possibly very different from those obtained in the steady approximation. This is for example the case of hydrogen explosions that can possibly breach the containment vessel of nuclear plants, a major concern during the week following the notorius Three Mile Island accident in the USA in 1979. Other example are given by the propagation of blast waves or the interaction of unsteady shock waves with the boundary layer over airplane wing, that may possible lead to shock-induced boundary layer separation. The numerical simulation of two-dimensional supersonic problems with strong moving shocks can be particularly challenging since, even with simple geometries, very complex unsteady

flows can develop [25]. A quite common feature of such flows is the presence of discontinuities in the variables separating regions where the flow is substantially uniform. To reduce the computational burden and improve the overall accuracy of the solution, mesh adaptation techniques can be adopted to increase the grid spacing only where it is required [1]. In the present work a Finite-Volume solver for the Arbitrary Lagrangian-Eulerian (ALE) formulation of the Euler equations over two-dimensional adaptive grids [6] is adopted to perform unsteady flow computations. The interpretation of the grid modifications as a continuous deformation of the finite volumes, resulting in a modification of the interface velocities, allows to compute the solution onto the new grid simply integrating the governing equations, without any explicit interpolation step [12].

GRID ALTERATION STRATEGY

The goal of grid alteration procedures is to locally modify the grid spacing so that the numerical error is evenly distributed within the elements of the computational domain. Therefore, according to the principle of error equidistribution, nodes will be inserted in the regions where the error is greater than the domain average, or deleted where it is smaller.

Since the exact value of the error is obviously unknown, the numerical error E has to be locally estimated. In most applications, error estimators are either functions of gradient or undivided differences [2, 9, 14, 17], or functions of the Hessian matrix $\mathcal{H}$ [3,9,10,16,24,26] of a convenient sensor variable which is representative of the flow features and whose choice depends on the physical problem. In the present study, to cope with the presence of shock waves and smooth-flow regions, the following Mach based nodal estimator is used

$$E_i = h_i^2 \sqrt{E_i^2(\boldsymbol{m}_\tau, M) + E_i^2(\boldsymbol{m}_n, MZ)},$$

with

$$E_i(\boldsymbol{m}, M) = \frac{\boldsymbol{m}^{\mathrm{T}} \mathcal{H}(M) \boldsymbol{m}}{h_i\, \boldsymbol{m}^{\mathrm{T}} \boldsymbol{\nabla} M + 0.12\, \mu(M)} + \frac{\boldsymbol{m}^{\mathrm{T}} \boldsymbol{\nabla} M}{h_i^3\, \boldsymbol{m}^{\mathrm{T}} \boldsymbol{\nabla} M + 0.12\, \mu(M) h_i} \tag{1}$$

The discrete Hessian matrix and the gradient vector are computed using a finite-element approximation within the node-pair representation [7,19]. Equation (1) is a modification of the error estimator proposed by Webster [24].

A triangular element is marked for refinement if the error is larger than a given threshold, e.g. $\frac{1}{3}\sum_i \mu(E_i(M)) + 0.1\sigma(E_i(M))$, where the sum is performed amongst the element nodes. Conversely, the grid-coarsening threshold is set equal to $0.98\mu(E(s))$, to force grid adaptation towards a greater uniformity in error distribution. The adopted elements refinement and nodes removal techniques are shown in figure 1.

In order to improve the grid quality, standard edge-swapping and grid smoothing techniques are also adopted [20]. A minimum size for the triangles is imposed in order to limit the number of nodes/elements close to flow discontinuities and, conversely, a maximum size chosen to limit the coarsening of uniform flow regions.

In order to perform unsteady computations with adaptive grids the following predictor-corrector method is used. At a given time level t_n a first-order accurate (in space) prediction of the solution is computed from the known values of the solution. The grid adaptation procedure is then carried out, based on the error estimated with computed prediction. A higher-order solution is then calculated at the time t_{n+1} over the new adapted grid. An area-based error interpolation technique is also implemented to allows more the one adaptation passage, i.e. allowing for more elements/nodes to be inserted/removed at each time step.

EDGE-BASED SOLVER FOR ADAPTIVE GRIDS

The Euler equations in an Arbitrary Lagrangian Eulerian (ALE) framework [4, 5] for compressible two-dimensional flows read

$$\frac{d}{dt}\int_{\mathcal{C}(t)} \mathsf{u} + \oint_{\partial\mathcal{C}(t)} \big[\mathbf{f}(\mathsf{u}) - \mathsf{u}\,\boldsymbol{v}\big]\cdot\boldsymbol{n} = 0, \qquad \forall \mathcal{C}(t) \subseteq \Omega(t), \tag{2}$$

System (2) is made complete by specifying suitable initial and boundary conditions [8]. The flux function is is defined as $\mathbf{f}(\mathsf{u}) = \big(\boldsymbol{m},\ \boldsymbol{m}\otimes\boldsymbol{m}/\rho + P(\mathsf{u})\,\mathsf{I}^2,\ \big[E^{\mathrm{t}} + P(\mathsf{u})\big]\,\rho/\boldsymbol{m}\big)^{\mathrm{T}}$ and the term $\mathsf{u}\,\boldsymbol{v} = (\rho\boldsymbol{v}, \boldsymbol{m}\otimes\boldsymbol{v}, E^{\mathrm{t}}\boldsymbol{v})^{\mathrm{T}}$ accounts for the flux contribution due to the movement of the control volume.

The finite volume discrete counterpart of the Euler equation (2) is obtained by selecting a finite number of non overlapping volumes $\mathcal{C}_i(t) \subset \Omega(t)$. In the node-centered approach considered here, each cell surrounds a single node i of the triangulation of Ω, as shown in figure 2. Over each finite volume, equation(2) reads

$$\frac{d[V_i\,\mathsf{u}_i]}{dt} = -\sum_{k\in\mathcal{K}_{i,\neq}} \int_{\partial\mathcal{C}_{ik}} \big[\mathbf{f}(\mathsf{u}) - \mathsf{u}\,\boldsymbol{v}\big]\cdot\boldsymbol{n} - \int_{\partial\mathcal{C}_i\cap\partial\Omega} \big[\mathbf{f}(\mathsf{u}) - \mathsf{u}\,\boldsymbol{v}\big]\cdot\boldsymbol{n}, \tag{3}$$

Where unknown vector is approximated over the cell by its average value $\mathsf{u}_i = \mathsf{u}_i(t)$. In equation (3) the sum is performed over the finite volumes $\mathcal{C}_k$ that share a portion of their boundary with $\mathcal{C}_i$, i.e. $\partial\mathcal{C}_{ik} = \partial\mathcal{C}_i \cap \partial\mathcal{C}_k \neq \emptyset$, thus the set corresponding set of indexes is $\mathcal{K}_{i,\neq} = \{k \in \mathcal{K} : k \neq i | \partial\mathcal{C}_i \cap \partial\mathcal{C}_k \neq \emptyset\}$, see

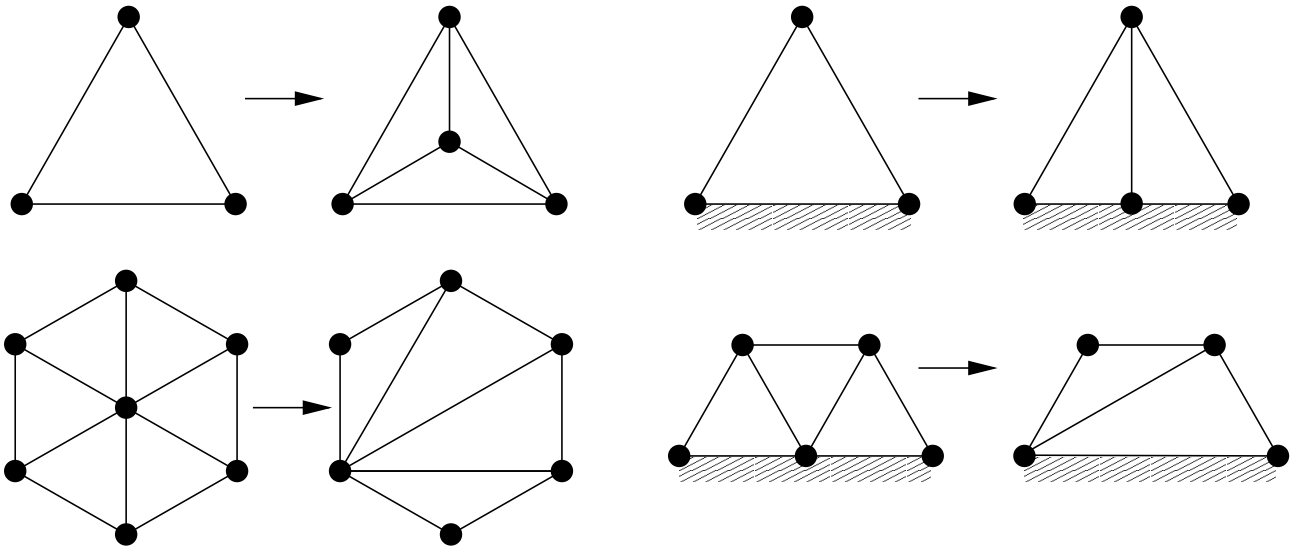

Figure 1. Top: refinement pattern by node insertion in the center of mass of an existing element for a domain (top-left) element and boundary (top-right) element. Bottom: Derefinement pattern by node deletion for a domain (bottom-left) element and boundary (bottom-right) element.

figure 2. The second term of the right hand side of equation (3), i.e. $\partial\mathcal{C}_i \cap \partial\Omega$, is given by the boundary contribution, if any. Each contribution of equation (3) has to be approximated with a suitable integrated normal numerical flux, representing the exchange across the cell interface [13]. E.g. a centered approximation of the domain fluxes gives

$$\Phi(\mathsf{u}_i, \mathsf{u}_k, \nu_{ik}, \boldsymbol{\eta}_{ik}) = -\frac{\mathbf{f}(\mathsf{u}_i) + \mathbf{f}(\mathsf{u}_k)}{2} \cdot \boldsymbol{\eta}_{ik} + \frac{\mathsf{u}_i + \mathsf{u}_k}{2}\, \nu_{ik}, \tag{4}$$

where the integrated normal vector and the integrated normal interface velocity are defined as

$$\boldsymbol{\eta}_{ik}(t) = \int_{\partial\mathcal{C}_{ik}} \boldsymbol{n} \qquad \text{and} \qquad \nu_{ik}(t) = \int_{\partial\mathcal{C}_{ik}} \boldsymbol{v}\cdot\boldsymbol{n}. \tag{5}$$

Equations (5)(left) and (5)(right) are consistency conditions that have to be exactly satisfied.

Moreover, by assuming a constant interface flux along the interface, the boundary integral in equation (3) simplifies to

$$\Phi^{\partial}(\mathsf{u}_i, \nu_i, \boldsymbol{\xi}_i) = -\mathbf{f}(\mathsf{u}_\partial(\mathsf{u}_i)) \cdot \boldsymbol{\xi}_i + \mathsf{u}_\partial(\mathsf{u}_i)\, \nu_i, \tag{6}$$

where the consistency conditions are

$$\boldsymbol{\xi}_i(t) = \int_{\partial\mathcal{C}_i\cap\partial\Omega} \boldsymbol{n} \qquad \text{and} \qquad \nu_i(t) = \int_{\partial\mathcal{C}_i\cap\partial\Omega} \boldsymbol{v}\cdot\boldsymbol{n}, \tag{7}$$

In the presented computations the numerical flux function of equation (4) is replaced by a Total Variation Diminishing (TVD) numerical flux [13, 21]. To this purpose, a flux limiter approach has been followed and the second order centered approximation is replaced by the first order Roe flux near flow discontinuities [18]. The switch is controlled by the limiter proposed by van Leer [21]. The above high-resolution version of the scheme requires the definition of an extended edge data structure that includes also the extension nodes $i^\star$ and $k^\star$, that are needed in the evaluation of the limiter function. As done by Ref. [23], the extension nodes belong to the two edges best aligned with i-k.

When dealing with moving/deforming meshes in the ALE framework an additional constrain is usually enforced to prevent spurious oscillations to appear in the solution. Such constrain is expressed as a conservation equation for the cell volumes termed Geometric Conservation Law (GCL) that can be automatically satisfied if the integrated velocities are computed as the derivatives of the volumes swept by the corresponding interfaces, i.e.

$$\nu_{ik}(t) = \frac{dV_{ik}}{dt} \qquad \text{and} \qquad \nu_i(t) = \frac{dV_{i,\partial}}{dt}. \tag{8}$$

A more general version of equation (3) for adaptive

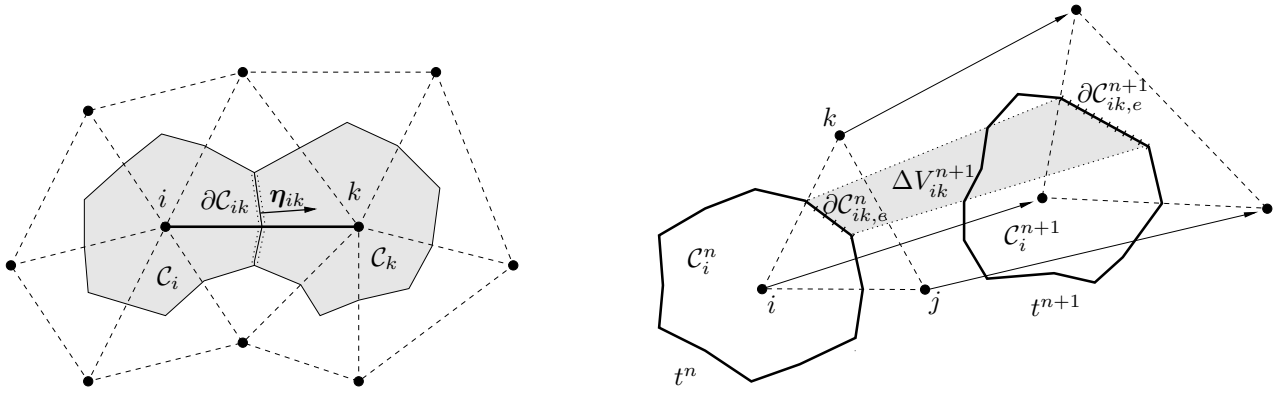

Figure 2. Left: edge associated with the finite volume interface $\partial\mathcal{C}_{ik} = \partial\mathcal{C}_i \cap \partial\mathcal{C}_k$ and metric vector $\boldsymbol{\eta}_{ik}$ in two spatial dimensions. The two shaded regions are the finite volumes $\mathcal{C}_i$ and $\mathcal{C}_k$; dashed lines indicate the underlying triangulation. Right: area swept by portion of the interface $\partial\mathcal{C}_{ik,e}$ pertaining to element e, made of nodes i, j and k, during the time interval $[t^n, t^{n+1}]$.

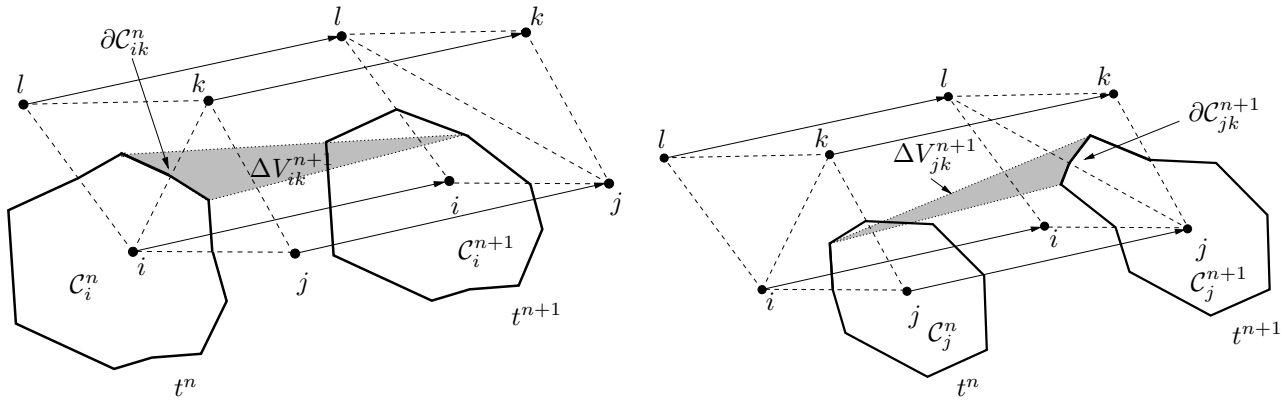

Figure 3. Interpretation of the edge swapping as continuous finite volume deformation. Left: evaluation of the normal interface velocity (area of the shaded region) for edge i-k that is deleted due to edge-swapping from edge i-k at time t^n into edge j-k at time t^{n+1}. Right: evaluation of the normal interface velocity for edge j-k that is created due to edge-swapping.

grids is given by

$$\begin{cases} \dfrac{d}{dt}[V_i\,\mathsf{u}_i] = \displaystyle\sum_{k\in\mathcal{K}_{i,\neq}(t)} \Phi(\mathsf{u}_i, \mathsf{u}_k, \nu_{ik}, \boldsymbol{\eta}_{ik}) \\ \qquad\qquad + \Phi^{\partial}(\mathsf{u}_i, \nu_i, \boldsymbol{\xi}_i), & \forall i \in \mathcal{K}(t) \\ \dfrac{dV_{i,ik}}{dt} = \nu_{ik}\,, & \forall k \in \mathcal{K}_{i,\neq}(t) \\ \dfrac{dV_{i,\partial}}{dt} = \nu_i\,, \end{cases} \tag{9}$$

where both the number of nodes, $\mathcal{K}$, and the connectivity, $\mathcal{K}_{i,\neq}$, may vary during the the computations. The ODE system above is solved using a Backward Differences Formulæ (BDF) scheme of order either one or two, as reported in the numerical results section. At each time level, a dual time-stepping technique is used to solve the non linear system of equations for the vector unknown at time $n+1$ [22].

The numerical scheme outline above is used together with mesh adaptation techniques. The local changes in grid topology, e.g. edge-swapping and node insertion/deletion, are interpreted as a continuous deformation of the finite volumes associated to the grid. As an example, in figure 3 the geometrical interpretation of edge-swapping in a continuous framework is sketched. The interface velocities given of equation (8) are thus computed taking into account the distortion of the finite volumes caused by such modifications. The solution onto the new, adapted, grid can therefore be computed simply integrating Eq. (9) without any explicit interpolation step. Additional flux contributions

must be taken into account for every removed edge [15] and additional conservation equations must be integrated for every removed node [12] in order to ensure the conservativity of the resulting scheme. Such additional fluxes and equations can be dropped after a given number of time steps depending on the time-integration scheme adopted, e.g. two for a BDF2 and three a BDF3, since their contribution is identically equal to zero. The reader is referred to [11, 12] for a detailed description of the ALE interpretation of grid adaptation.

NUMERICAL RESULTS

In the present section numerical results obtained with the scheme outlined above are shown. The selected test case is the forward-facing step made famous by Woodward and Colella [25]. Supersonic conditions are imposed at the inlet, i.e. $M = 3$, slip conditions are imposed on the lower and upper boundaries of the duct and no conditions are imposed at the outlet. The gas is ideal and polytropic with a heat capacity ratio of 1.4. The initial solution is uniform and correspond to the one imposed at the inlet, namely $P = 1.0$, $\boldsymbol{v} = (3, 0)^{\mathrm{T}}$ and $\rho = 1.4$.

Two different computations have been carried out: a reference one with a uniform fixed grid of 48,324 points (95,618 triangles) and an adaptive one with an initial grid of 7,603 points (14,799 triangles). The minimum allowed size for the adaptive case is set to be 0.005 mesh units, which is roughly twice the spacing of the fixed grid. To better capture the less intense flow-field features, e.g. rarefaction fans or weak shocks, the modified Webster error estimator of equation (1) is adopted together with a multi-passage approach [14] with two levels. The governing equations are integrated in time resorting to a second order BDF scheme for the fixed grid case and a backward Euler scheme for the adaptive one. The non-dimensional time-step is equal to 1/300 corresponding to a maximum Courant number of 1.67 in the fixed grid case and 2.67 in the adaptive one.

In the figures 4–7 the density distribution obtained with the adaptive grid is compared with the one computed on the fixed grid and a reference solution [25]. The adapted mesh is also shown for different values of non-dimensional time. In both the fixed and the adapted computations the front curved shock is very well captured and it appears to be sharper than the shock of the reference case. In the adapted case however the weaker shocks are not sufficiently highlighted by the sensor: for example the upper portion of the shock in figure and the discontinuity reflected by the lower boundary in figures and are significantly diffused.

Even though the rarefaction fan is only slightly captured by the adaptation scheme, the overall solution does not seem to be penalized. Indeed, in all the presented cases, both the front and the reflected shocks are curved due to the interaction with the expansion fan.

As a final remark it has to be noted that the adapted grid computations resulted to be ten times faster than the fixed grid ones on a single core machine. Moreover the total number of nodes required in the adaptive computation varies from 14% to 25% of the nodes required in the fixed case. The proposed approach, thus, allows to significantly decrease the computational costs with a similar level of accuracy.

CONCLUSION

An automatic mesh adaptation technique, coupled with an Arbitrary Lagrangian Eulerian description of the flow equations, was used to simulate the unsteady flow field around the forward-facing step, a standard CFD test case proposed by Woodward and Colella [25]. The flow field features a strong curved shock propagating upstream and interacting with the upper wall, where a lambda shock is eventually observed. The adapted-grid solution compares fairly well with reference results and with a fixed fine grid computation. The computational time required by the adapted-grid technique is is roughly one order of magnitude smaller than that required by the fixed-grid computation, thus confirming the suitability of the present approach to simulate the dynamics of strong shocks. The weaker shock waves reflecting at the upper boundary are less resolved than the stronger ones, which feature higher gradients of the solution. The adoption of a multi-passage technique with three levels should help to better capture such weaker shocks.

REFERENCES

1. M. Darbandi A. Naderi and M. Taeibi-Rahni. Developing a unified fve-ale approach to solve unsteady fluid flow with moving boundaries. *International Journal for Numerical Methods in Fluids*, 63(1):40–68, 2010.
2. T.J. Baker. Mesh adaptation strategies for problems in fluid dynamics. *Finite Elements Analysis and Design*, 25:243–273, 1997.
3. M.J. Castro-Diaz, F. Hect, B. Mohammad, and O. Pironneau. Anisotropic unstructured mesh adaptation for flow simulations. *Int. J. Numer. Meth. Fluids.*, 25:475–491, 1997.
4. J. Donea. An arbitrary Lagrangian-Eulerian finite element method for transient fluid–structure interactions. *Comp. Meth. Appl. Mech. Engng.*, 33:689–723, 1982.
5. J. Donea, A. Huerta, J.-Ph. Ponthot, and A. Rodríguez-Ferran. Arbitrary Lagrangian-Eulerian methods. In R. Stein, E. de Borst, and T.J.R. Hughes, editors, *The Encyclopedia of Computational Mechanics*, volume 1, chapter 14, pages 413–437. Wiley, 2004.
6. G. Forestieri, D. Isola, F. Marulli, G. Quaranta, and A. Guardone. Numerical simulation of compressible vortical flows using a conservative unstructured-grid adaptive scheme. In *2nd European Seminar on Coupled Problems*, June 28^{th}–July 2^{nd} 2010.
7. M. Fossati, A. Guardone, and L. Vigevano. An edge-based

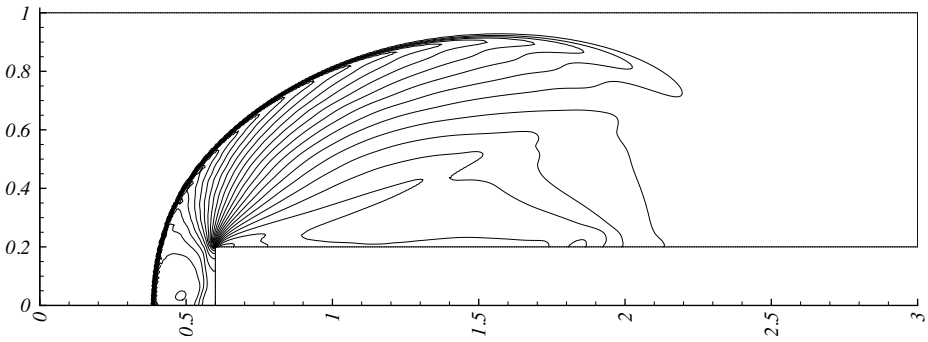

(a) Density contours, fixed

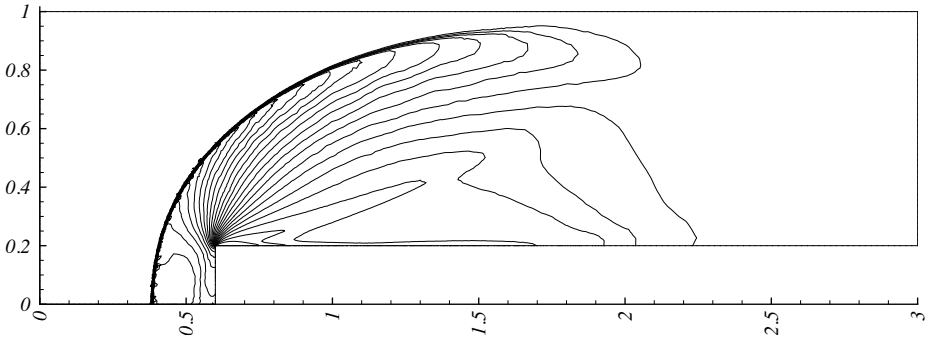

(b) Density contours, adapted

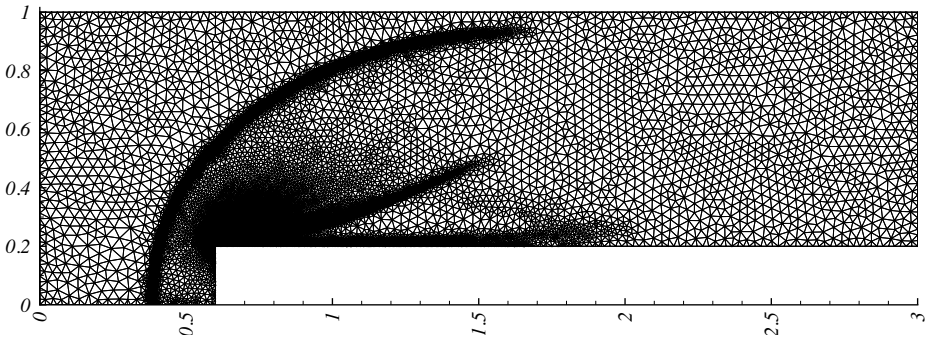

(c) Grid, adapted

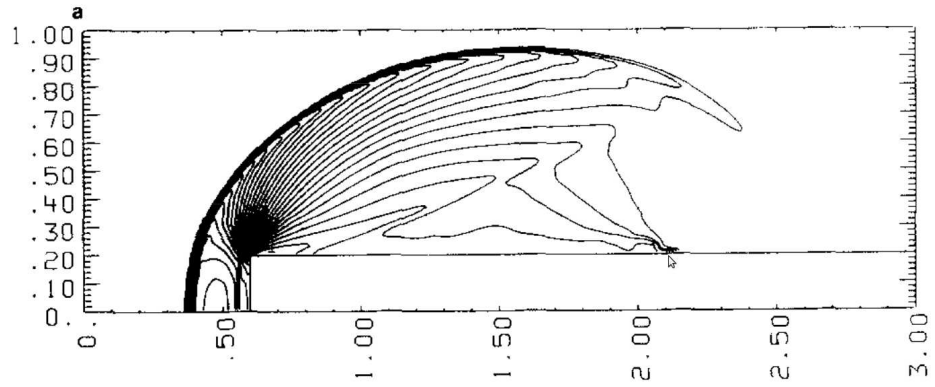

(d) Density contours, reference

Figure 4. Comparison of the density contours with the fixed grid computations and the reference [25] and computational grid at the non-dimensional time 0.500543.

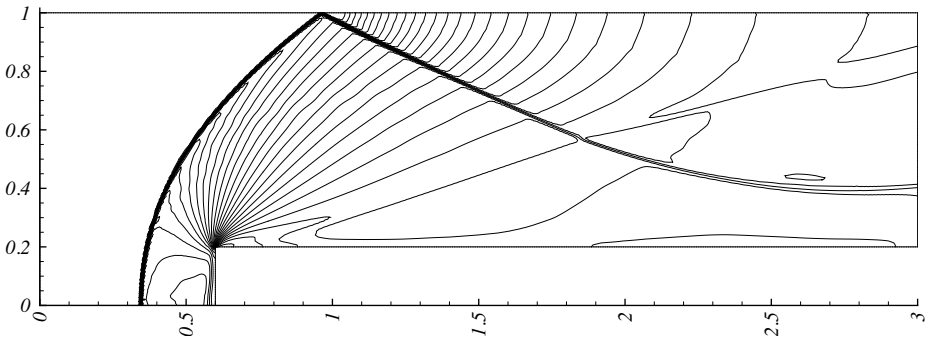

(a) Density contours, fixed

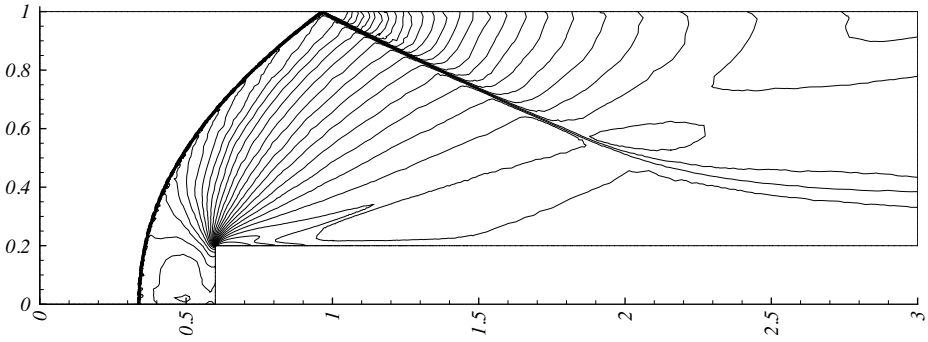

(b) Density contours, adapted

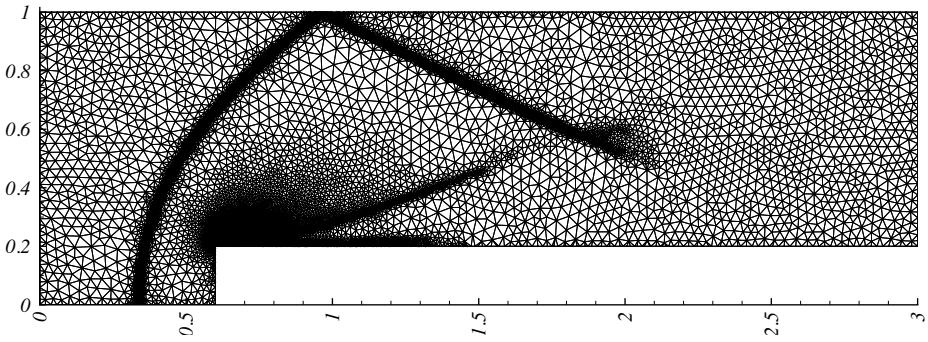

(c) Grid, adapted

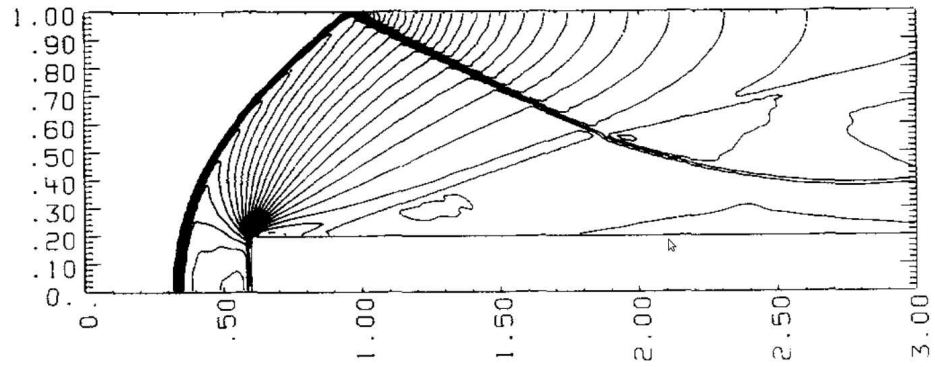

(d) Density contours, reference

Figure 5. Comparison of the density contours with the fixed grid computations and the reference [25] and computational grid at the non-dimensional time 1.00044.

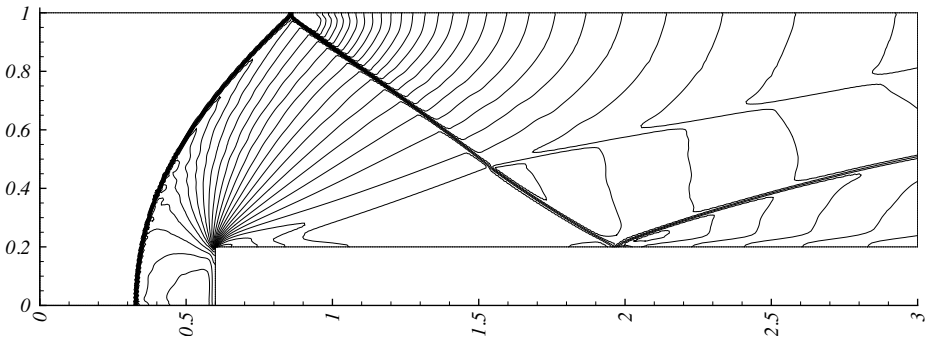

(a) Density contours, fixed

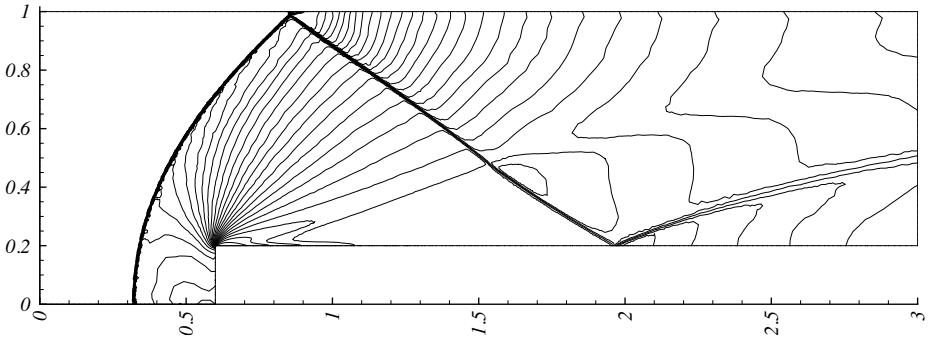

(b) Density contours, adapted

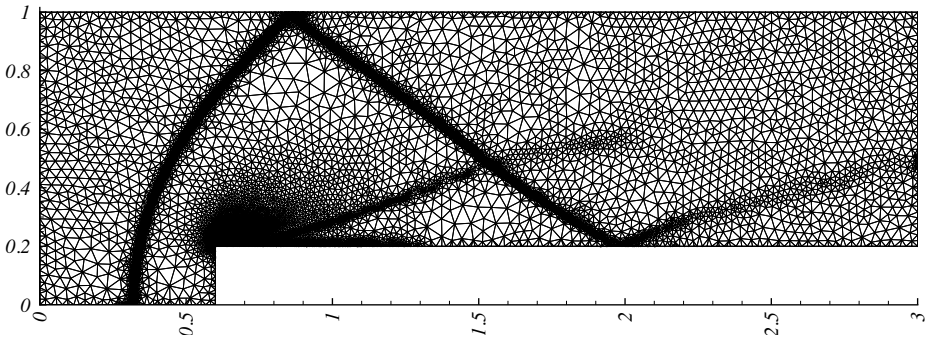

(c) Grid, adapted

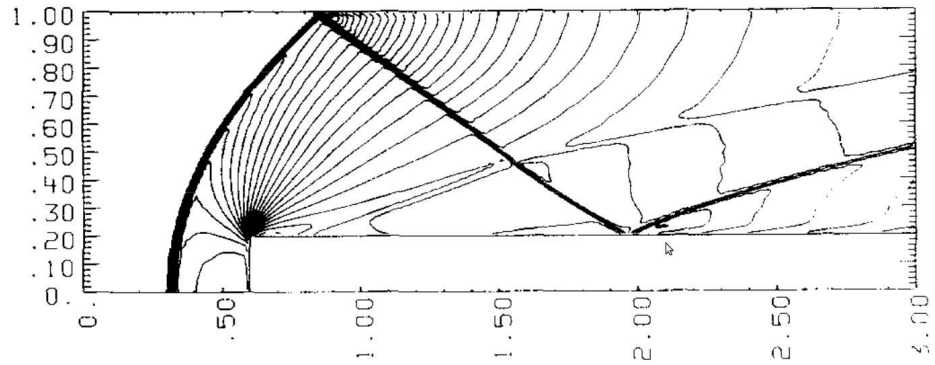

(d) Density contours, reference

Figure 6. Comparison of the density contours with the fixed grid computations and the reference [25] and computational grid at the non-dimensional time 1.50285.

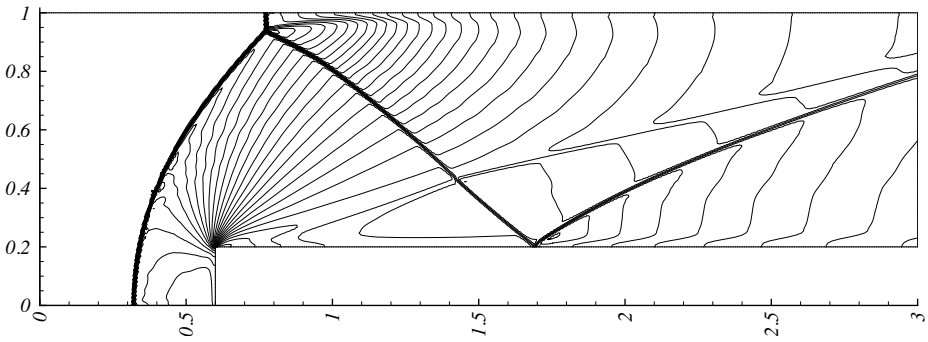

(a) Density contours, fixed

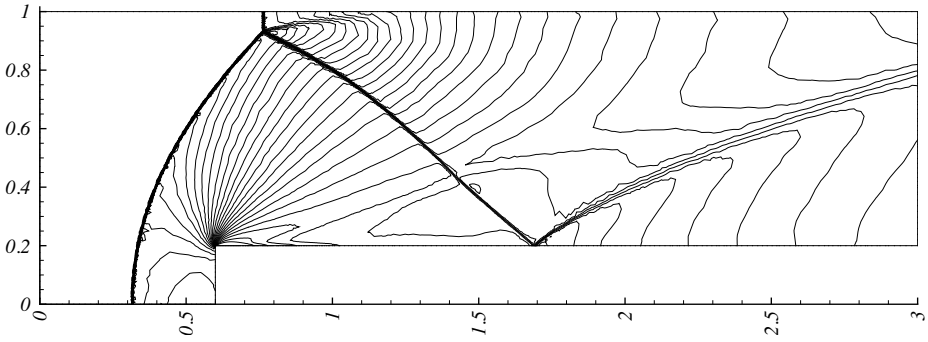

(b) Density contours, adapted

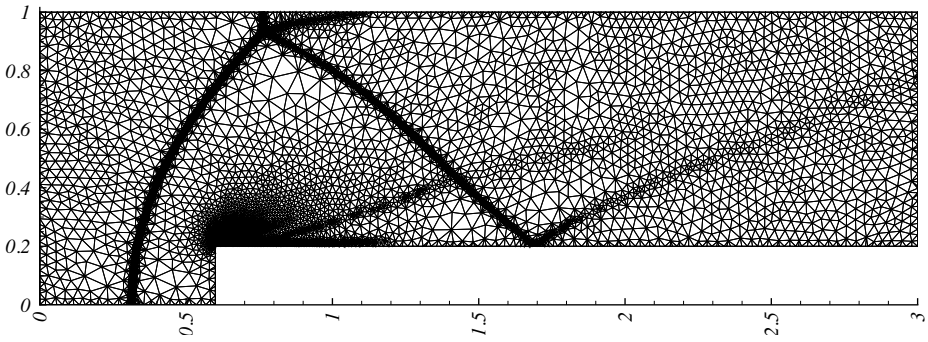

(c) Grid, adapted

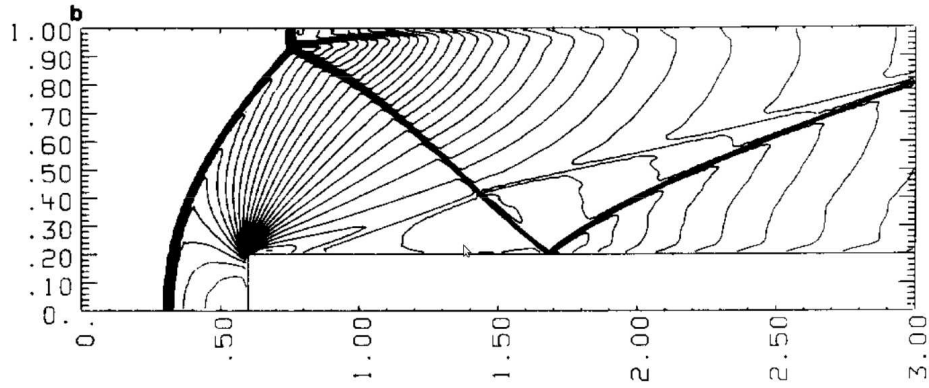

(d) Density contours, reference

Figure 7. Comparison of the density contours with the fixed grid computations and the reference [25] and computational grid at the non-dimensional time 2.00456.

mesh adaption technique for two-dimensional compressible flows on unstructured grids. In *Proceeding of the XIX Congresso Nazionale AIDAA*, Forlì, September 17–21 2007. AIDAA.
8. E. Godlewski and P. A. Raviart. *Numerical approximation of hyperbolic systems of conservation laws*. Springer-Verlag, New York, 1994.
9. G.P.Warren, W.K. Anderson, J.T. Thomas, and S.L.Krist. Grid convergence for adaptive methods. In *AIAA 10^{th} Computational Fluid Dynamics Conference*, 1991. AIAA Paper 91-1592.
10. H.G. Habashi, J. Dompierre, Y. Bourgault, D. Ait-Ali-Yahia, M. Fortin, and M.G. Vallet. Anisotropic mesh adaptation: towards user-indipendent, mesh indipendent and solver-indipendent CFD. Part I: General principles. *Int. J. Num. Meth. Fluids*, 32(6):725–744, 2000.
11. D. Isola, A. Guardone, and G. Quaranta. Arbitrary lagrangian eulerian formulation for grids with variable topology. In E. Oñate M. Papadrakakis B. Schrefler, editor, *Proceedings of the III Int. Conf. on Computational Methods for Coupled Problems in Science and Engineering ECCOMAS COUPLED PROBLEMS 2009*. CIMNE, Barcelona, 2009.
12. D. Isola, A. Guardone, and G. Quaranta. An ale scheme without interpolation for moving domain with adaptive grids. In *40th Fluid Dynamics Conference and Exhibit, AIAA*, 2010.
13. R. J. LeVeque. *Finite volume methods for conservation laws and hyperbolic systems*. Cambridge University Press, 2002.
14. R. Lohner. Mesh adaptation in fluid mechanics. *Engineering Fracture Mechanics*, 50:819–847, 1995.
15. D. Muffo, G. Quaranta, and A. Guardone. Compressilbe fluid-flow ale formulation on changing topology meshes for aeroelastic simulations. In *Proceedings of the* 26^{th} *ICAS Congress*, Anchorage, Alaska, September 14–19 2008.
16. J. Peraire, M. Vadhati, K. Morgan, and O.C. Zienkiewicz. Adaptive remeshing for compressible flow computations. *J.Comput. Phys.*, 72:449–466, 1987.
17. S. Pirzadeh. Unstructured viscous grid genereration by the advancing layers method. *AIAA J.*, 32(8):1735–1737, 1994.
18. P. L. Roe. Approximate Riemann solvers, parameter vectors, and difference schemes. *J. Comput. Phys.*, 43:357–372, 1981.
19. V. Selmin. The node-centred finite volume approach: bridge between finite differences and finite elements. *Comp. Meth. Appl. Mech. Engng.*, 102:107–138, 1993.
20. J. F. Thompson. *Numerical grid generation: foundations and applications*. Elsevier Science Publishing, 1985.
21. B. van Leer. Towards the ultimate conservative difference scheme II. Monotonitic and conservation combined in a second order scheme. *J. Comput. Phys.*, 14:361–370, 1974.
22. V. Venkatakrishnan and D. J. Mavriplis. Implicit method for the computation of unsteady flows on unstructured grids. *J. Comput. Phys.*, 127:380–397, 1996.
23. N. P. Weatherill, O. Hassan, M. Marchant, and D. Marcum. Adaptive inviscid solutions for aerospace geometries on efficiently generated unstructured tetrahedral meshes. AIAA Paper 93-3390, 1993.
24. B.E. Webster, M.S. Shepard, Z. Rhusak, and J.E. Flaherty. Automated adaptive time discontinuous finite element method for unsteady compressible airfoil. *AIAA J.*, 32:748–757, 1994.
25. P. Woodward and P. Colella. The numerical simulation of two-dimensional fluid flow with strong shocks. *J. Comput. Phys.*, 54:114–173, 1984.
26. G. Xia, D. Li, and C. L. Merkle. Anisotropic grid adaptation on unstructured meshes. In *39^{th} Aerospace Sciences Meeting and Exhibit*, 2001. AIAA Paper 2001-0443.